EFDA–JET–PR(10)25

F. Nabais, D. Borba, M. Garcia-Muñoz, T. Johnson, V.G. Kiptily, M. Reich,
M.F.F. Nave, S.D. Pinches, S.E. Sharapov and JET EFDA contributors

Impact of Strongly Driven Fishbones and Alfvén Eigenmodes on Fast Ion Losses

Impact of Strongly Driven Fishbones and Alfvén Eigenmodes on Fast Ion Losses

F. Nabais[1], D. Borba[1], M. Garcia-Muñoz[2], T. Johnson[3], V.G. Kiptily[4], M. Reich[2], M.F.F. Nave[1], S.D. Pinches[4], S.E. Sharapov[4] and JET EFDA contributors*

JET-EFDA, Culham Science Centre, OX14 3DB, Abingdon, UK

[1]Associação EURATOM/IST, Instituto de Plasmas e Fusão Nuclear – Laboratório Associado, Instituto Superior Técnico, P-1049-001 Lisboa
[2]MPI für Plasmaphysik, EURATOM Association, Garching, Germany
[3]EURATOM-VR Association, Alfvén Laboratory, Royal Institute of Technology, 10044 Stockholm, Sweden
[4]EURATOM-CCFE Fusion Association, Culham Science Centre, OX14 3DB, Abingdon, OXON, UK
** See annex of F. Romanelli et al, "Overview of JET Results", (Proc. 22 nd IAEA Fusion Energy Conference, Geneva, Switzerland (2008)).*

Preprint of Paper to be submitted for publication in
Nuclear Fusion

ABSTRACT

The instabilities responsible for ICRH accelerated fast ion losses in plasmas with monotonic profile of the safety factor and long period sawteeth, as well as the range of energies at which the losses occur, were identified on the JET tokamak. The temporal evolution of fast ion losses with resolution on energy and pitch angle was measured using the scintillator probe, which allows to determine the orbits of the fast ions that reach the detector. On the other hand, the orbits of the fast ions in resonance with Alfvénic instabilities were identified using the CASTOR-K code, so it is possible to identify which instabilities were responsible for the losses collected in the detector. Two different phases of losses, with different characteristics, were identified. The first phase occurs just after a sawtooth crash, when TAE and high frequency fishbones are unstable. In this phase, TAE are responsible for most of the measured losses. Losses caused by fishbones, if any, are not significant. The second phase initiates when tornado modes (TAE inside the q=1 radius) become unstable: the peak loss signal increases by a factor of 2 to 5, the average energy of the ions that reach the detector decreases and its pitch angle increases. In this phase, the strong drive of the tornado modes by the ICRH accelerated ions initiates the losses.

1. INTRODUCTION

The loss of fast ions from the plasma may have significant detrimental effects on the operation of future tokamaks. It may cause the auxiliary heating to be inefficient [1] or, in case of alpha particles leaving the plasma, fusion burn may not be self-sustained. Moreover, lost ions can also cause severe damage to the tokamak walls [2] [3]. In the case of ITER for example, the first wall can only tolerate losses at very low level before suffering damage [4]. For these reasons, the study of fast ion losses in tokamaks acquires a considerable relevance and dedicated experiments have been carried out in several machines. In JT-60U, energetic particle confinement studies have been carried out by measuring the neutron emission rate derived from the nuclear reaction between high energy protons (E>3MeV) and boron ions [5] and by measuring neutral particle fluxes [6]. Measurements of alpha particle losses induced by MHD during DT experiments carried out in TFTR have been described in reference [7]. In JET, experimental studies on the effect of MHD instabilities and Alfvénic modes on the confinement of energetic particles in the advanced tokamak scenario have been reported in [8],[9]. In JET monotonic scenario, previous observation and modelling of fast ion loss [10] have been done based on measurements of the γ-rays emitted through their inelastic scattering with carbon impurities, since diagnostics measuring direct losses were not available at that time. To allow further exploration of the physics of fast ion loss, fast ion loss detectors [11,12] have been installed in JET and it is possible now to undertake dedicated experiments.

In JET experiments with monotonic profile of the safety factor q, several instabilities known to cause radial displacement of the fast ions are commonly observed, like fishbones [13,14,15], Toroidal Alfvén Eigenmodes (TAE) [16] and tornado modes (core-localized TAE inside the q=1 surface) [17]. A set of experiments was carried out in order to identify which of these instabilities

are able to efficiently expel fast ions from the plasma in this type of scenario. Aside from identifying the sources of the losses, it is also important to determine the range of energies at which the losses could occur, as well as identify on which factors their number and energies depend. To improve the experimental results, it is desirable that a large population of highly energetic ions is driven. According to the Stix model [18], the fast ion temperature of an Ion Cyclotron Resonance Heating (ICRH) driven population is proportional to the volume-averaged ICRH power density applied to the plasma and inversely proportional to the plasma density, $T_{HOT} \sim \langle P_{ICRH} \rangle \tau_{slow}/n_{HOT}$, where n_{HOT} is the fast ion density and τ_{slow} is the fast ion slowing down time, which is inversely proportional to the plasma density. This suggests the use of high ICRH powers and low plasma densities, thus the "grassy sawteeth scenario" [19] was an adequate choice. This scenario is obtained by applying a high power, H minority, on-axis Ion Cyclotron Resonance Heating on a low density Deuterium plasma (see figure 1). No NBI is used, except for diagnostic purposes. When the plasma density is above the threshold for grassy sawteeth, very long periods (sometimes longer than one second) without sawtooth crashes are normally observed [15], which allow a large population of fast ions to build up and a variety of instabilities to develop. Under these conditions, high frequency precessional drift fishbones [13], hybrid fishbones [15], low frequency diamagnetic fishbones [14], TAE [16] and tornado modes [17] are usually observed [15]. This scenario is then ideal to determine the tendency of these instabilities to expel fast ions from the plasma.

The main tool to analyse the losses of fast ions from the plasma is the scintillator probe diagnostic [11,12] recently installed at JET [20], which allows measuring both the gyro-radius and the pitch angle of the lost ions that reach the scintillator plate. The scintillator plate is located at the edge of the plasma on the low field side below the midplane (see figure 2) and is able to detect fast ions moving in orbits of the type of the one depicted in the same figure. The range of gyro-radius and pitch angle on which the scintillator probe is able to detect lost ions is defined by the slit geometry and the magnetic field. The scintillator cup operates as a magnetic spectrometer delivering data with resolution of 5% in pitch angle and 20% in gyro-radius at a sampling rate of 20Hz and having an integration time of 50ms. The energy of the detected ions can then be calculated from the gyro-radius, $r = \sqrt{2mE_{\perp}/B_T Z}$ (m is the mass, $E_{\perp}$ the perpendicular energy, B_T the toroidal magnetic field and Z the electric charge), while the normalized form of the magnetic momentum, which is best adequate to describe ICRH generated populations, can be calculated from the measured angle, $\Lambda \equiv \mu B_0/E = B_0/B)1\text{-}\cos^2 q$).Here μ is the magnetic momentum, B is the magnetic field measured at the scintillator cup, B_0 is the magnetic field on axis and q is the measured pitch angle.

The orbits of the fast ions are usually defined by three invariants of the motion: the energy E, the magnetic momentum μ and the toroidal canonical momentum P_ϕ. As referred, by convenience, we use here $\Lambda \equiv \mu B_0/E$, which is also an invariant, instead of μ. The advantage of this is that an approximation of the whole ICRH driven fast ion population can be described by a single value of Λ, due to the characteristics of the Ion Cyclotron Resonance Heating [21]. Each set of invariants (E, Λ, P_ϕ) then defines uniquely an orbit, except for some cases in which two orbits can exist for

the same set of invariants. In this case, it is necessary to use an additional index σ to distinguish them. Since two orbits characterized by the same set of invariants (E, Λ, P_ϕ) are necessarily nestled one enveloping the other, it is used σ=1 for the exterior orbit and σ=-1 for the interior one. Reference [22] provides figures which allow visualising the type of orbits corresponding to each set of invariants (E, Λ, P_ϕ). In the case of the lost ions detected by the scintillator probe, the pair (E, Λ) can be obtained directly from measurements, while the toroidal canonical momentum P_ϕ can be determined knowing the location of the probe. All lost ions move in banana orbits when they reach the scintillator probe (we set σ=1), so their orbits can be uniquely determined at the moment they reach the detector. The original orbits of the fast ions that interact with the different modes (and may eventually be lost) are identified using the CASTOR-K code [23]. This code receives as input the plasma equilibrium, the mode eigenfunction and the fast ions distribution function. The equilibrium is reconstructed by the codes EFIT [24] and HELENA [25], while the normal mode problem is solved numerically by the MISHKA code [26]. The fast ion distribution is written as a function of the invariants ($E, \Lambda, P_\phi; \sigma$), each set of values defining a different orbit. The distribution of the fast ions in energy is characterized by a temperature since the repeated heating of the fast ions accelerated in the same resonance causes the population to have an approximately Maxwellian energy distribution [22]. The fast ion temperature T_{HOT} to use as input in the CASTOR-K code can be determined experimentally by the gamma-ray diagnostics [27] or else can be calculated numerically by the PION [28] and SELFO [29] codes. Since the gamma-ray diagnostics measure a line-integrated temperature, they produce usually lower temperature measurements than those calculated by the PION and SELFO codes for the centre of the plasma. The CASTOR-K code allows the use of radial profiles of the fast ion temperature, with the parameter T_{HOT} referring to the value in the centre of the plasma. The normalized magnetic momentum Λ, as referred before, is approximated by a constant (Λ=1 for on-axis heating) while the distribution in P_ϕ, which is related to the radial location of the fast ions, corresponds to a fast ion population peaked in the centre of the plasma, being the parameters defining this distribution adjustable. The CASTOR-K code is then able to calculate the resonant transference of energy between the fast ions and the mode [30]

$$\delta W_{HOT} = -\frac{2\pi^2}{\Omega m^2} \sum_\sigma \int dE d\mu dP_\varphi \tau_b (\omega - n\omega_*) \frac{\partial F}{\partial E} \sum_{p=-\infty}^{\infty} \frac{|Y_p|^2}{\omega + n\langle\dot{\varphi}\rangle + p\omega_b}$$

where,

$$Y_p = \oint \frac{d\tau}{\tau_b} L^{(1)} e^{ip\omega_b \tau} \text{ and } \omega_* = \frac{\partial F/\partial P_\varphi}{\partial F/\partial E}.$$

ω_b and τ_b are the bounce frequency and bounce time respectively, Ω is the gyro-frequency, j is the toroidal coordinate, $F(E, \Lambda, P_\phi; \sigma)$ is the unperturbed fast ion distribution function and $L^{(1)}$ is the linearized perturbed Lagrangian. Since this calculation is done for each orbit separately, it allows identifying which particles from the original fast ion distribution are resonant with the mode. This paper is organized as follows: In section 2 we present the details of the experiments and the

experimental results. In section 3 we describe the modelling carried out and the numerical results. These results and their comparison with experimental findings are discussed and summarized in section 4, where conclusions are also drawn.

2. EXPERIMENTAL RESULTS

In the scenario of high ICRH power and on-axis H minority heating applied on a low density D plasma (see figure 1), when the plasma density is above the threshold for grassy sawteeth, long period sawteeth occur and a variety of MHD activity is observed between sawtooth crashes (see figure 3). During this period, two different phases of losses have been identified, the length of each of them depending strongly on the ICRH power. At high ICRH power (P_{ICRH} ~ 6-7MW) each phase lasts roughly half of the sawtooth period while in pulses with lower ICRH power (P_{ICRH} ~ 4-5MW) the second phase is significantly shorter. Regarding the species of ions that reached the scintillator probe, only H ions were detected between sawtooth crashes (during sawtooth crashes D ions were also detected) and all energies of lost ions throughout the text refer to H ions (D ions have different energies for the same gyro-radius). This was expected since the fast ion population interacting with the instabilities was composed by the H ions accelerated by ICRH. During the first phase, the instabilities normally observed are TAE, precessional drift fishbones and hybrid fishbones. The fast ion losses manifest as an outspread "cloud" in the 2-dimensional phase space covered by the scintillator probe, with energies that range approximately from 600eV to above 3.25MeV and angles that range from 50 degrees to 80 degrees (see figure 4). Λ=1 (characterizing banana orbits with tips on the magnetic axis) corresponds approximately to the angle of 65 degrees. Higher angles correspond to banana orbits with tips on the low field side while lower angles correspond to banana orbits with tips on the high field side. We note that although the heating was applied on axis, most of the ions collected by the scintillator probe were moving in banana orbits with tips slightly shifted to the high field side (pitch angles below 65 degrees, corresponding to Λ<1). The intensity of the loss signal increases towards the centre of the "cloud", with the maximum of losses occurring for angles between 60 and 65 degrees and for energies around 1.9MeV. In the second phase, TAE, diamagnetic fishbones and tornado modes are usually unstable. When the transition from the first phase to the second phase occurs, the peak loss signal increases by a factor of 2 to 5 and the loss distribution in the phase space becomes narrower. There is also a clear change in the location of the "cloud" of losses (see figure 5) corresponding to changes of the average values of the energies and pitch angles of the ions that reach the detector. The pitch angles increase, ranging now from 60 degrees to 80 degrees, and the energies decrease, now ranging from 1.2MeV to 2.4MeV. The peak loss signal is now located at around 70 degrees and 1.7MeV.

3. MODELLING AND INTERPRETATION

3.1 MODELLING

The identification of the instabilities causing the loss of fast ions is complicated by the fact that

there is normally more than one of them unstable at any time. To identify which of these instabilities cause resonance interaction with fast ions of interest, the CASTOR-K code [23] was used. This code calculates the resonant transference of energy between a fast ion population and a given mode for each orbit individually, which allows to identify the orbits of the fast ions in resonance with that mode, being each orbit defined by a set invariants (E, Λ, P_ϕ). Since for a fast ion population generated by IRCH, $\Lambda \equiv \mu B_0/E$ can be approximated by a constant (for instance, $\Lambda=1$ in the case of on-axis heating), the results from the CASTOR-K code are presented graphically in a 2-dimensional plot on the space (E, P_ϕ), with Λ assuming the role of a parameter. The contour plot identifies then the orbits of the fast ions, characterized by the set $(E, 1, P_\phi)$, in resonance with the mode.

The resonant ions identified by the CASTOR-K code will then interact with the mode and their orbits will change. During this interaction, the magnetic momentum of the ion is conserved but the energy and the toroidal canonical momentum are allowed to change, with the change in energy being proportional to $(\omega/n)\Delta P_\varphi$, where ΔP_φ is the change in toroidal canonical momentum of the ion [3]. Since the frequency of the Alfvén waves is small when compared with the cyclotron frequency, the interaction implies predominantly a variation of the toroidal canonical momentum of the fast ions. The toroidal canonical momentum is defined by $P_\varphi = Ze\psi + (ZeR/q)n_\parallel B_\varphi$, where ψ is the poloidal magnetic flux, e is the electric charge, Z is the particle charge number, Ω is the gyro-frequency and B_ϕ is the toroidal magnetic field [23]. At the point where the parallel velocity of the ion changes sign ($v_\parallel=0$), this is, at the tip of the banana orbit, the toroidal canonical momentum reduces to the term proportional to the poloidal flux, $P_\varphi = Ze\psi$. Thus, the change in P_ϕ implies a change in ψ at the tip of the banana orbit, this is, the tip of the banana orbit moves over a vertical line (the tip of the banana orbit does not move horizontally because the magnetic momentum is conserved). When the ion is driving the mode, i.e. when there is transference of energy from the ion to the mode, the radial movement of the tip of the orbits is outward in the minor radius. Figure 6 shows schematically possible changes in the orbits of energetic ions interacting with a mode. A topological transition from potato orbit to banana orbit occurs when P_ϕ cross the threshold value (for $\Lambda = 1$ this threshold is $P_\phi = 0$). Tornado modes have a strong interaction with the energetic ions moving in orbits near the core while TAE interact with ions moving in orbits that reach closer from the edge. The combination of tornado modes inside the $q = 1$ surface and TAE outside may cause a fast ion to drift over a significant distance in the plasma. The CASTOR-K doesn't allow predicting the final position of a fast ion after interacting with a mode, it only allows identifying which fast ions are exchanging energy with the mode. Thus, modelling alone does not allow predicting if an ion moving in a given orbit is going to leave the plasma. However, since the energy exchanged is relatively small, if the loss of fast ions is being caused by resonant interaction with the modes, the range of energies at which the CASTOR-K code predicts interaction to occur must fit the range of energies measured experimentally of the fast ions reaching the scintillator plate. Aside from this, fast ions experiencing a weak interaction with the mode may also leave the plasma if they are moving in orbits that reach close from the plasma edge. In this case, just a small drift of the tip of its banana orbit may be enough to cause its loss.

3.2 TAE LOSSES

In the period that follows a giant sawtooth crash, a broad pattern of losses is observed. During this period, TAE and precessional drift or hybrid fishbones are normally unstable, all of those, instabilities being known to be able to cause a radial outward drift of fast ions. We remind that hybrid fishbones initially behave exactly like precessional drift fishbones and they differ only after the frequency chirp down. While precessional drift fishbones eventually vanish, hybrid fishbones change their behaviour, and its frequency continue chirping down. Thus, using a high frequency as input in the CASTOR-K code, it will allow to model both precessional drift fishbones and hybrid fishbones at their high frequencies. Note that fishbones at their higher frequency interact with fast ions with higher energies and consequently moving in larger orbits, easier to be lost from the plasma. The experimental finding of a lack of changes in the loss signal as measured by the scintillator probe when precessional drift fishbones were replaced by hybrid fishbones suggests that no further modelling needs to be done for lower frequencies. The frequency chosen to be used as input in the CASTOR-K code was then around the fishbones' initial frequency (70 kHz). The eigenfunction for the internal n=1 kink mode, which is a good approximation for fishbones, was calculated by the MISHKA code and is shown in figure 7. The fast ion temperatures in the plasma centre calculated by the PION and SELFO codes were around 1 MeV for pulse #66380 and 500 keV for pulse #66378. The line integrated temperatures measured by the gamma-ray diagnostics for the same pulses were approximately 500 keV for pulse #66380 and 250 keV for pulse #66378. Numerical simulations with the CASTOR-K code were carried out for central fast ion temperatures of 500 keV and 1 MeV with the dependence of the fast ion losses on the fast ion temperature being discussed in section IV. Using $\Lambda \equiv \mu B_0/E = 1$ and a radial distribution of the fast ion population peaked in the centre, the CASTOR-K code was then used to calculate the resonant exchange of energy between the fast ion population and the high frequency (70kHz) fishbones as a function of (E, P_ϕ). Here "high frequency fishbones" refer both to the precessional drift fishbones and the hybrid fishbones, and the results obtained for $T_{HOT} = 500$keV are presented in figure 8 (top). The orbits of the ions that interact with the instability correspond to the blue zones in the phase space (E, P_ϕ), with darker blue meaning a more intense interaction. Reading (E, P_ϕ) from this figure and adding $\Lambda = 1$, we recover the set (E, Λ, P_ϕ) necessary to identify an orbit. Figure 9 (top) shows that the fast ions resonant with the high frequency fishbones are ions with energies below 1MeV moving in banana orbits close from the plasma core (see fig. 9, top). There is a second region of resonance corresponding to ions with energies between 1MeV and 1.6MeV moving in more peripheral orbits (see fig. 9, bottom), but this region is barely visible when the temperature of the fast ion population is $T_{HOT} = 500$keV. Carrying out more simulations with the CASTOR-K code with increased fast ion temperature (1MeV), it predicts the regions of resonance shown in figure 8 (bottom). It can be observed that the number of particles in the more peripheral resonance, which is now clearly visible, increases significantly but the energies of these particles do not. Thus, we predict that no significant interaction occurs between the high frequency fishbones (70 kHz) and fast ions with energies above 1.6 MeV (this threshold is

lower if lower frequencies are used as input in the CASTOR-K code). Since most of the lost ions collected in the scintillator plate have energies above this threshold, these results indicate that resonant interaction with fishbones is not the main cause of the broad pattern of losses occurring in the period that follows a sawtooth crash. During this period, TAE were also observed in the magnetic spectrograms, the higher amplitude modes having toroidal mode numbers from n=7 to n=10 both in pulse #66378 and in pulse #66380. TAE eigenfunctions were also calculated with the MISHKA code and an example of the typical eigenfunction of the TAE is presented in figure 10. Contrary to the fishbones case, whose eigenfunctions are localized in the plasma core, the TAE have high amplitudes in the plasma edge. Similar modelling was then carried out with the CASTOR-K code for the interaction between these modes (n = 7 to n = 10) and the same fast ion populations used previously for the fishbones case. The modelling predicts that TAE are able to interact with fast ions with energies of up to 4 MeV (there is also a resonance at around 6MeV), thus covering well the range of the detected lost particles' energies. To illustrate these results, the regions of resonance in the phase space (E, P_ϕ) obtained with the CASTOR-K code are presented in figure 11 for the n = 8 TAE (T_{HOT} = 500keV (top) and of T_{HOT} = 1MeV (bottom)). For modes with different toroidal mode numbers the results are similar with the regions of resonance slightly shifted in energy. In these figures, the interaction near the edge (high values of P_ϕ) may be underestimated due to limited number of poloidal harmonics of the eigenfunctions calculated by the MISHKA code. The orbits of the fast ions that maximize the resonant exchange of energy with the n = 8 TAE are shown in fig.12 for T_{HOT} = 500 keV (top) and for T_{HOT} = 1MeV (bottom). These are particles moving in large banana orbits, which reach close to the plasma edge during the outer leg of their trajectories.

3.3 TORNADO LOSSES

When tornado modes become unstable (tornado modes with toroidal mode numbers from n = 7 to n = 10 were observed before monster sawtooth crashes), the detected loss patterns change significantly: The scintillator footprint gets narrower, shifts to lower energies and higher pitch angles and the peak loss signal increases by a factor up to 5. The temporal correlation between the onset of tornado modes and the changes on the loss signature makes clear that these changes are due to the onset of tornado modes. As in the previous section, the eigenfunctions of tornado modes (n = 7 to n = 10) have been calculated with the MISHKA code. The eigenfunctions of these modes are composed by two consecutive poloidal harmonics and contrary to the TAE's, they are localized in the plasma core as can be seen in figure 13 for the case of the n = 9 mode. A modelling was then carried out with the CASTOR-K code for the interaction between the tornado modes and the same fast ion population used in the previous section. Numerical results for the case of the n=9 tornado mode showing the regions of resonance in the phase space (E, P_ϕ) obtained with the CASTOR-K code for fast ion temperatures of T_{HOT} = 500keV (top) and of T_{HOT} = 1MeV (bottom) are presented in figure 14. When the fast ion temperature is T_{HOT} = 500keV, the CASTOR-K code predicts that tornado modes interact both with fast ions moving in banana orbits and with fast ions moving in

potato orbits, these last maximizing the exchange of energy (see fig.15). For T_{HOT} = 1MeV, the interaction of tornado modes with fast ions moving in potato orbits is largely dominant. The orbits that maximize the exchange of energy for T_{HOT} = 1 MeV are the same as for T_{HOT} = 500 keV (see fig.15) The types of orbits of the ions interacting with tornado modes also depend on the toroidal mode number n, with particles moving in banana orbits being more relevant for modes with lower n. Of particular interest is the range of energies on which the fast ions are able to interact with tornado modes. If the losses are triggered by resonant interaction with tornado modes, then the range of energies on which the CASTOR-K predicts interaction between tornado modes and the fast ion population must cover the energies of the lost ions measured experimentally (1.2MeV to 2.4 MeV). The energies at which this interaction occurs depend on the toroidal mode number of the modes. In the cases of the n = 8 and n = 9 modes (the last one shown in fig. 14), a strong interaction occurs mostly for fast ions with energies up to around 2.5MeV, which is in good agreement with the energies of the lost ions measured experimentally. However, in case of the n = 7 and n = 10 modes the CASTOR-K predicts this interaction to extend to energies up to around 3MeV, energies at which fewer losses are observed. This suggests that a strong interaction between fast ions and tornado modes is not condition sufficient to cause the loss these ions. In summary, tornado modes are predicted to interact with fast ions with lower energies than those which interact with TAE, which explains the observed decrease in the energies of the lost ions measured experimentally.

SUMMARY, DISCUSSION AND CONCLUSIONS

In addition to the modelling presented in the last section, a detailed data analysis was also carried out. This allowed to compare directly some of the numerical results with the experimental results and to draw conclusions about the validity of the numerical modelling carried out. The analysis of data confirmed the predictions of the modelling regarding the identification of the instabilities responsible for fast ion losses was correct.

Two different phases of losses are observed in these experiments. The first phase is observed when TAE and precessional drift fishbones are normally unstable, the latter being eventually replaced by hybrid fishbones. Modelling the interaction between the ICRH driven fast ion population and the fishbone mode with a frequency near its initial value, 70kHz, it allowed to predict that fishbones do not interact with fast ions with energies above around 1.6MeV. Thus, fishbones can't be responsible for the large majority of the losses, which have been observed to occur at higher energies. At this frequency there are no differences between precessional drift and hybrid fishbones so the modelling holds for both, and at lower frequencies, fishbones interact with fast ions with lower energies. On the other hand, numerical modelling has shown that TAE can interact with fast ions belonging to a range of energies that fits well with the experimental measurements of the energies of the lost ions. The conclusion that fast ion losses in this phase are caused by TAE is confirmed by experimental observations. In Pulse No: 66378 (P_{ICRH} ~ 6MW), it occurred sometimes that hybrid fishbones were stabilized before tornado modes or diamagnetic fishbones were destabilized, creating a window

where only TAE were unstable. The signature of the losses generated by TAE alone could then be compared with the signature generated by TAE plus high frequency fishbones. No differences could be observed between the two signatures, allowing to conclude that if fishbones were responsible for any losses, they were hidden by the losses caused by TAE. Moreover, in the same pulse, there were periods of time after sawtooth crashes in which neither TAE nor fishbones were unstable. In these periods no losses could be measured above the detection limit, which confirms that the broad pattern of losses observed in this phase is effectively caused by TAE.

In the second phase, the pattern of losses narrows, changes to lower energies and the number of counts increases. The clear temporal correlation between the observed changes in the loss signature and the onset of tornado modes leaves no doubts that the changes in the loss signal are caused by these modes. The losses triggered by tornado modes do not replace the already existing losses caused by TAE but will generate an additional signal that overlaps the previous signal. This new pattern of losses is essentially shaped by the losses triggered by tornado modes since they are significantly more numerous than those caused by TAE. The "narrowing" of the loss pattern is an indication that the fast ion losses triggered by tornado modes come from a smaller area in the phase space (E, P_ϕ) than the previous losses associated with TAE, which is in agreement with numerical results.

Two different explanations have been presented in order to describe the losses of fast ions by tornado modes. One of them indicates that the resonant overlap of neighbouring resonances close to the prompt loss boundary is the responsible for the enhanced losses [10]. A second explanation attributes the losses to the combined action of modes sweeping across a portion of the plasma radius [31] and TAE. In this case, tornado modes would initiate the radial transport of fast ions from the core to the peripheral regions of the plasma. At this point, the eigenfunction of tornado modes overlaps the eigenfunction of TAE, both being Alfvénic modes with similar frequencies and similar toroidal mode numbers, and TAE would continue to diffuse the fast ions all the way to the plasma edge [32], in a process similar to the one described in ref. [33].

Another relevant conclusion is that the number of lost ions measured by the scintillator probe depends strongly on the ICRH power but the energies of the lost ions do not. This can be easily explained since losses are measured at the energies at which the fast ions resonate with the modes and the resonance condition do not depends on the ICRH power. However, increasing the ICRH power, the number of fast ions with energies sufficiently high to verify this condition increases, resulting in enhanced losses.

ACKNOWLEDGMENTS

This work, supported by the European Communities under the contract of Association between EURATOM/IST, was carried out within the framework of the European Fusion Development Agreement. '' Financial support was also received from ''Fundação para a Ciência e Tecnologia'' and ''Programa Operacional Ciência, Tecnologia, Inovação do Quadro Comunitário de Apoio III.''. The views and opinions expressed herein do not necessarily reflect those of the European Commission.

REFERENCES

[1]. H.H. Duong *et al.,* Nuclear Fusion, **33**, 749 (1993)

[2]. R. White *et al.,* Physics of Plasmas, **2**, 2871, (1995)

[3]. W.W. Heidbrink, Physics of Plasmas, **15**, 055501, (2008)

[4]. ITER Physics Basis Expert Group on Energetic Particles, Heating and Current Drive, ITER Physics Basis Editors: Chapter 5: Physics of energetic ions, 1999 Nuclear Fusion **39** 2471

[5]. H. Kimura *et al.,* Nuclear Fusion, **38**, 1303 (1998)

[6]. K. Shinohara *et al.,* Nuclear Fusion, **42**, 942 (2002)

[7]. S. J. Zweben *et al.,* Nuclear Fusion, **39**, 1097, (1999)

[8]. Sharapov S. E. *et al.,* Nuclear Fusion, **45**, 1168, (2005)

[9]. Sharapov S. E. *et al.,* Nuclear Fusion, **46**, S868, (2006)

[10]. S.D. Pinches *et al.,* Nuclear Fusion, **46**, S904 (2006)

[11]. S. Baumel *et al.,* Review of Scientific Instruments, **75**, 3563, (2004)

[12]. D. Darrow *et al.,* Review of Scientific Instruments, **77** 10E701, (2006)

[13]. L. Chen, R. White and M. Rosenbluth, Physical Review Letters, **52** 1122 (1984)

[14]. B. Coppi and F. Porcelli, Physical Review Letters, **57**, 2272 (1986)

[15]. F. Nabais *et al.,* Physics of Plasmas, **12**, 10, 102509, (2005)

[16]. K.L. Wong, Plasma Physics and Controlle Fusion, **41**, R1, (1999)

[17]. G. Kramer *et al.,* Physical Review Letters, **83** 1122 (1999)

[18]. T. H. Stix, Nuclear Fusion **15**, 737 (1975)

[19]. M. Mantsinen et al. Plasma Physics and Controlle Fusion **42**, 1291, (2000)

[20]. M. Reich et al. 34th EPS Conference on Plasma Physics, Warsaw, Poland, 2-6 July 2007, http://epsppd.epfl.ch/Warsaw/pdf/O4_016.pdf

[21]. B. Coppi S. Migliuolo and F. Porcelli, Physics of Fluids **31**, 1630 (1988)

[22]. R. White, "The Theory of Toroidally Confined Plasmas", Imperial College Press, London (2001)

[23]. D. Borba and W. Kerner, Jouurnal of Computational Physics **153**, 101 (1999)

[24]. L. L. Lao *et al.,* Nuclear Fusion, **25**, 1661 (1985)

[25]. L. G. Huysmans *et al.,* Physics of Fluids B **5**, 1545 (1993)

[26]. A. B. Mikhailovskii *et al.,* Plasma Physics Reports **10**, 844 (1997)

[27]. V.G. Kiptily *et al.,* Nuclear Fusion, **42** 999, (2002)

[28]. L-G. Eriksson, T. Hellsten and U. Willén, Nuclear Fusion **33**, 1037 (1993)

[29]. J. Hedin, T. Hellsten, L.-G. Eriksson, T. Johnson, Nuclear Fusion, **42**, 527 (2002)

[30]. F. Porcelli *et al.,* Physics of Plasmas, **1** (3), 470 (1994)

[31]. H.E. Mynick and N. Pomphrey, Nuclear Fusion **34**, 1227 (1994)

[32]. S. Bernabei *et al.,* Physics of Plasmas **6**, 1880 (1999)

[33]. Garcia-Munoz, M. et al, PRL, 100, 055005 (2008)

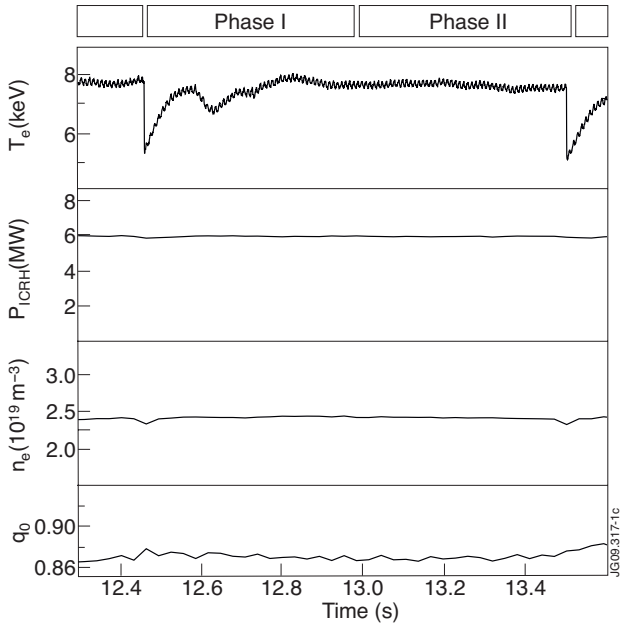

Figure 1: Electron temperature, ICRH power, central electron density and safety factor on axis during a monster sawtooth in the "grassy sawteeth scenario", I_p= 2.5MA, B_t=2.7 T. The two phases of losses are identified on the top.

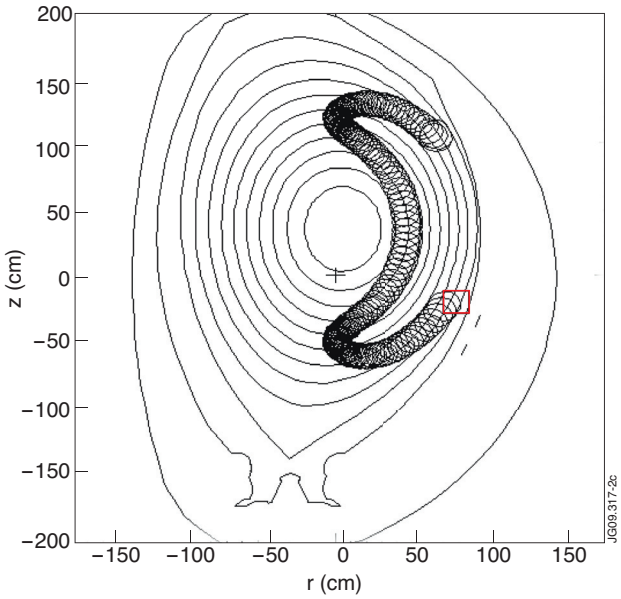

Figure 2: Location of the scintillator plate (red box) and typical orbit of a lost ion before it reaches the scintillator plate. This example corresponds to a 2.5MeV H ion with pitch angle= 64 degrees ($\Lambda \approx 0.98$).

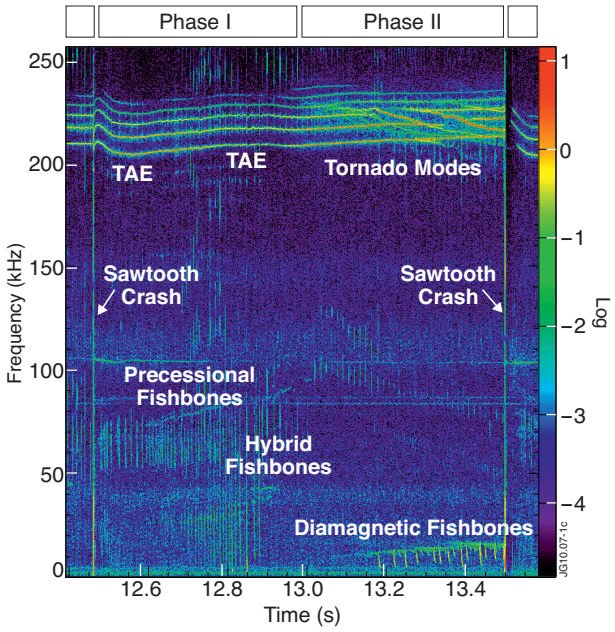

Figure 3: Typical spectrogram of MHD activity detected with the Mirnov coils for the period between two monster sawtooth crashes in the "grassy sawteeth scenario" (Pulse No: 66378). The two phases of losses are identified on the top.

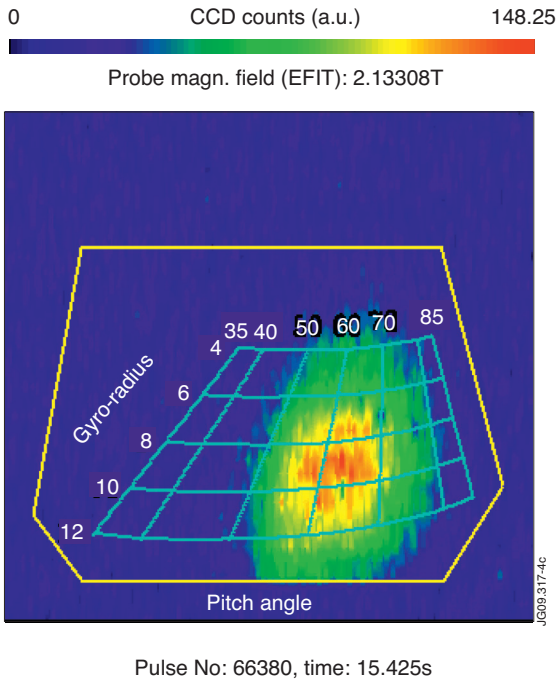

Figure 4: Footprint of the fast ion losses measured by the scintillator probe in the phase in which TAE and precessional drift fishbones are unstable. Correspondence Gyro-radius to Energy: 4cm = 0.535MeV, 6cm = 0.925MeV, 8cm = 1.499MeV, 10cm = 2.25MeV, 12cm = 3.18MeV.

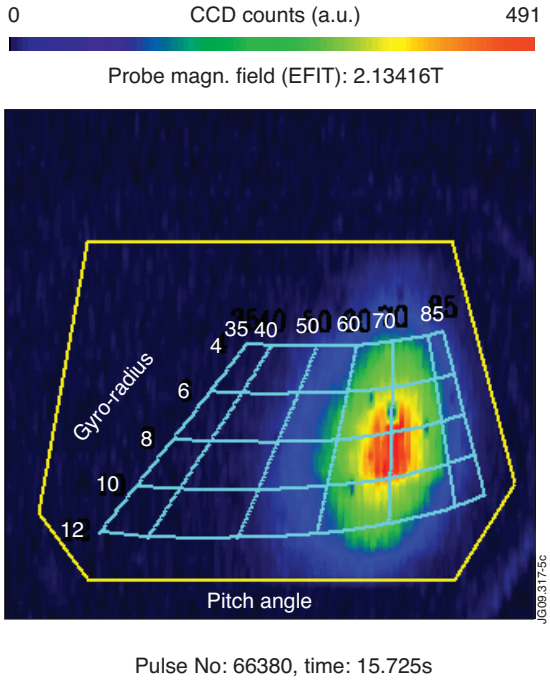

Figure 5: Footprint of the fast ion losses measured by the scintillator probe in the phase in which tornado modes, TAE and diamagnetic fishbones are unstable. Correspondence Gyro-radius to Energy: 4cm = 0.535MeV, 6cm = 0.925MeV, 8cm = 1.499MeV, 10cm = 2.25MeV, 12cm = 3.18MeV.

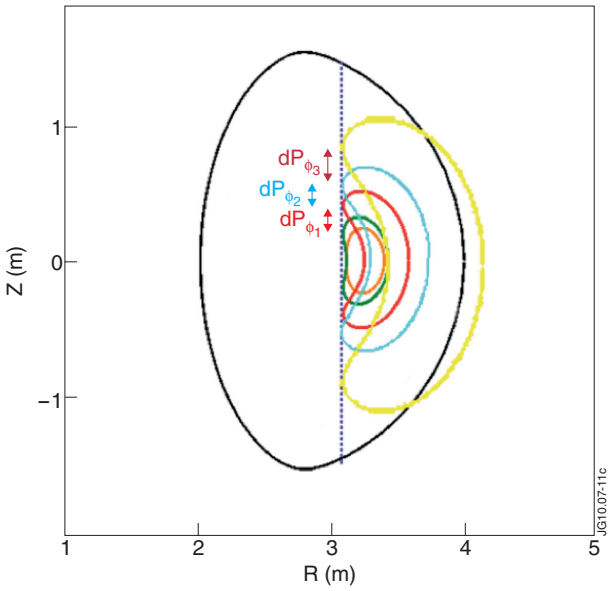

Figure 6: Schematics of the change in the shape of the orbits of energetic ions when the ions transfer energy to a mode.

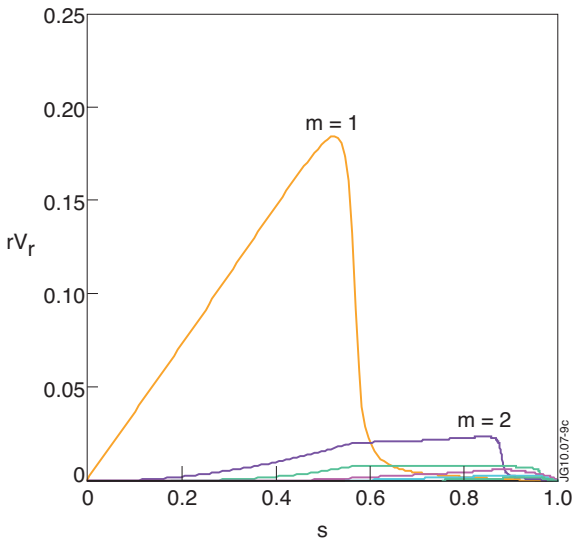

Figure 7: Eigenfunction calculated by MISHKA code used as input in the CASTOR-K code for the fishbone instability (n=1).

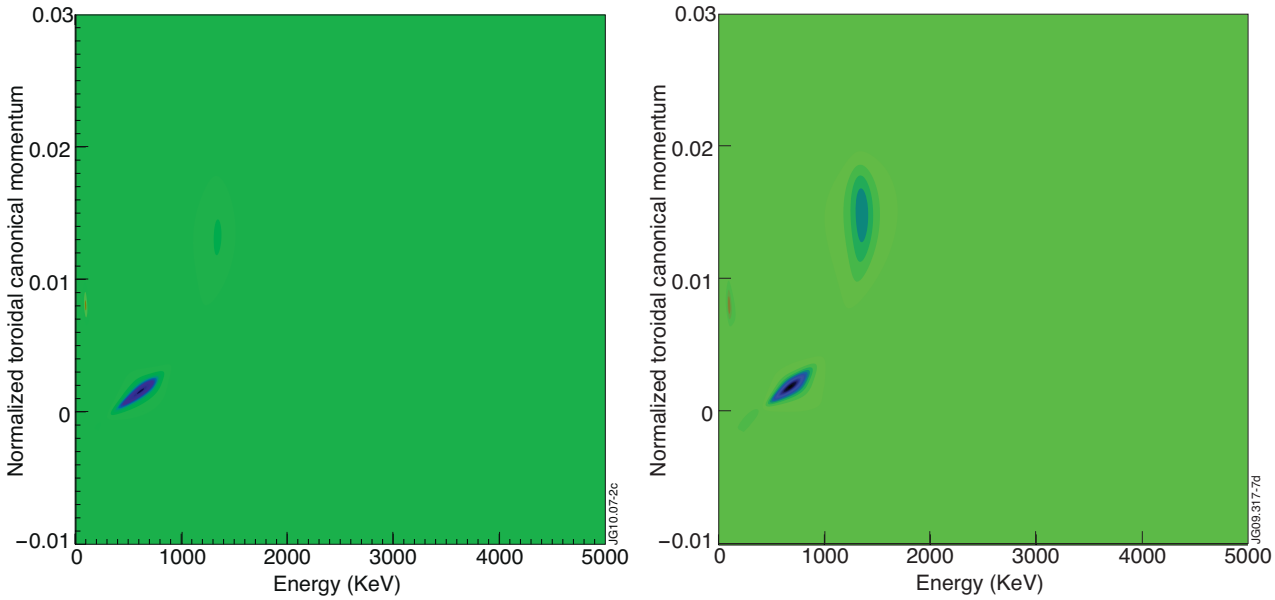

Figure 8: Energy exchanged by the high frequency fishbones and the ICRH driven fast ion population as a function of P_ϕ/ψ_1 and E with Λ=1. ψ_1 is the poloidal flux at the edge of the plasma. Top: T_{HOT} = 500keV, Bottom: T_{HOT}= 1MeV.

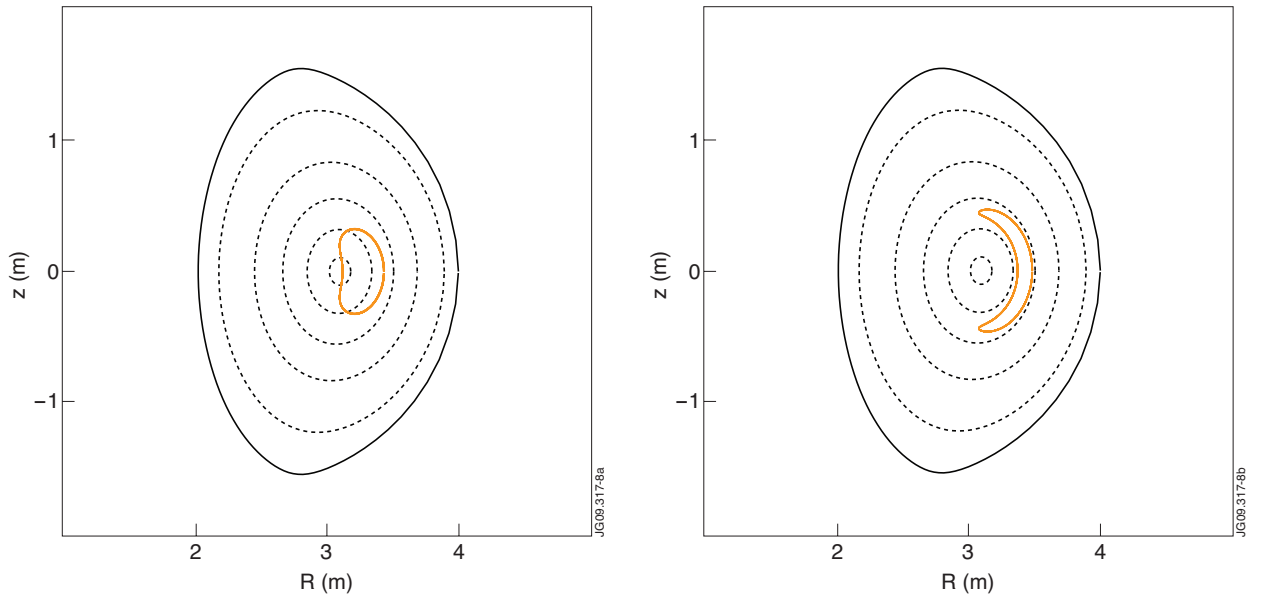

Figure 9: Poloidal projection of the orbits that experience a stronger interaction with the high frequency fishbones. Top: Orbit corresponding to the main region of resonance (E ≈ 620keV, $P_\phi/\psi_1 \approx 0.0015$ and $\Lambda = 1$). Bottom: orbit corresponding to the weaker region of resonance (E ≈ 1.35 MeV, $P_\phi/\psi_1 \approx 0.015$ and $\Lambda = 1$).

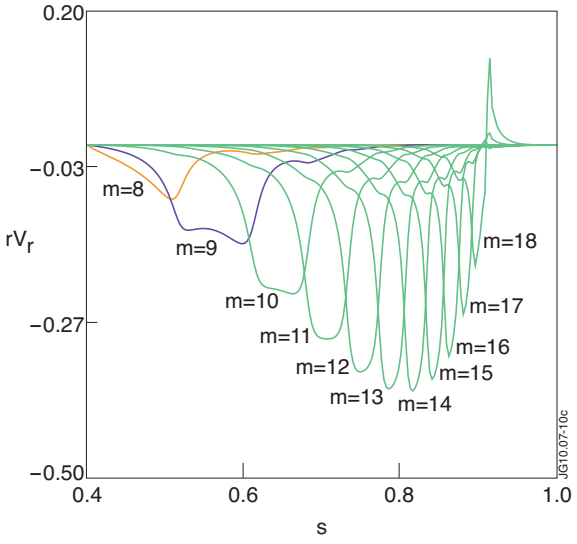

Figure 10: Eigenfunction calculated by MISHKA code used as input in the CASTOR-K code for the n=8 TAE.

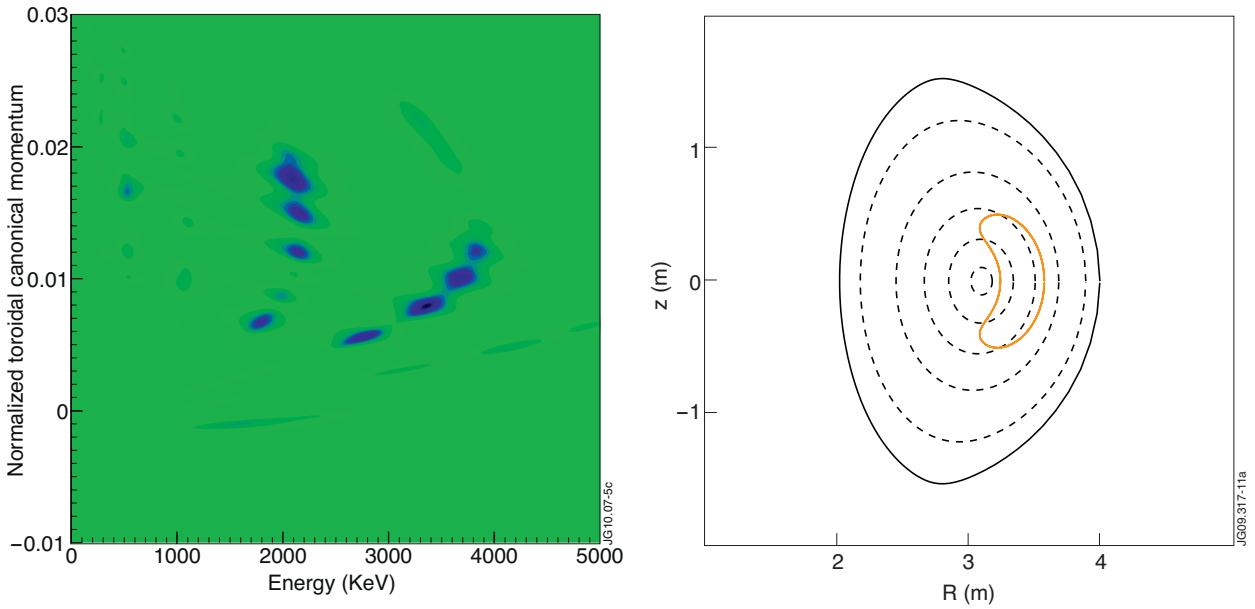

Figure 11: Energy exchanged by the n = 8 TAE and the ICRH driven fast ion population as a function of P_ϕ/ψ_1 and E with Λ=1. ψ_1 is the poloidal flux at the edge of the plasma. Top: T_{HOT} = 500keV, Bottom: T_{HOT} = 1MeV.

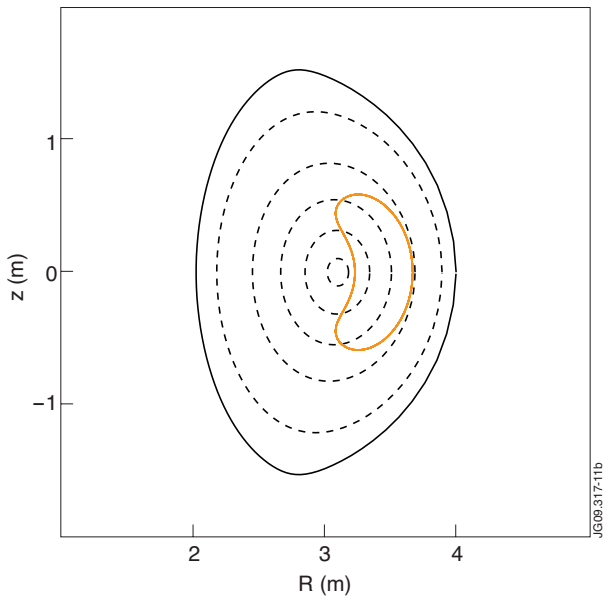

Figure 12: Poloidal projection of the orbits that experience a stronger interaction with the n = 8 TAE. Top: T_{HOT} = 500 keV, orbit defined by ($E \approx 1.8$MeV, $P_\phi/\psi_1 \approx 0.0075$ and $\Lambda = 1$). Bottom: T_{HOT} = 1MeV orbit defined by ($E \approx 3.35$ MeV, $P_\phi/\psi_1 \approx 0.008$ and $\Lambda = 1$).

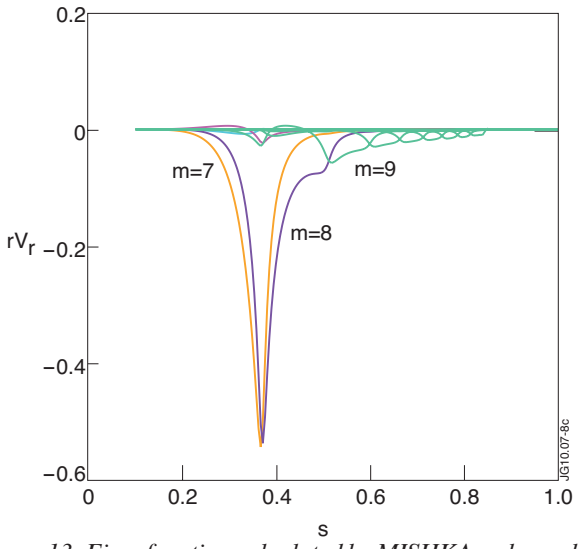

Figure 13: Eigenfunction calculated by MISHKA code used as input in the CASTOR-K code for the n = 9 tornado mode.

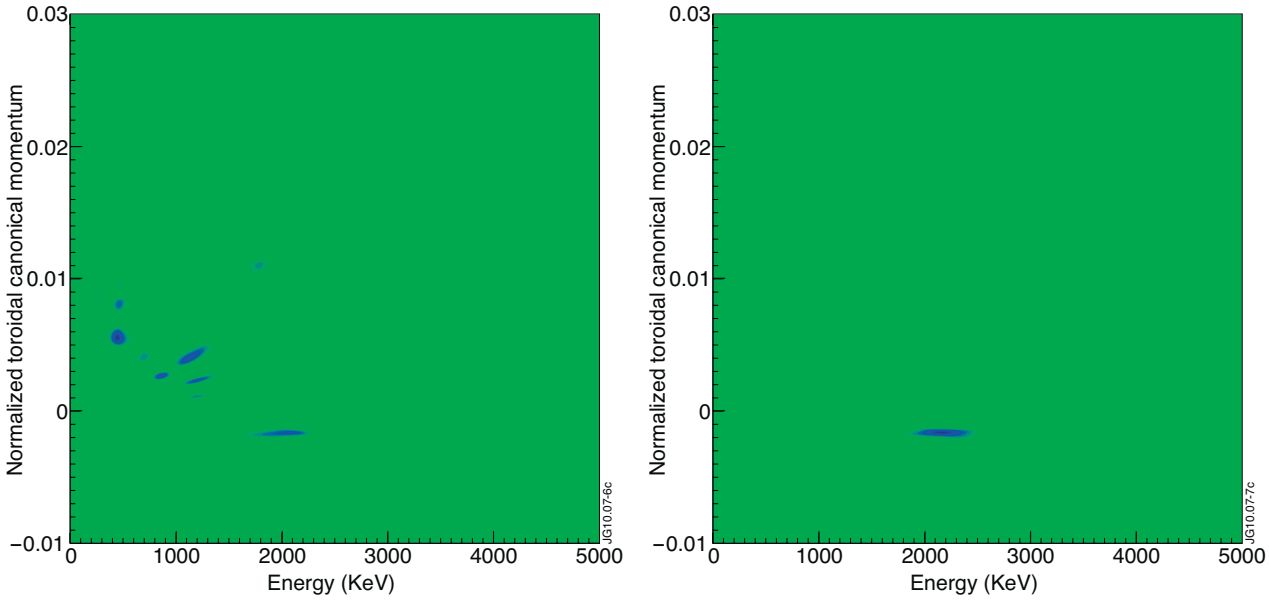

Figure 14: Energy exchanged by the n=9 tornado mode and the ICRH driven fast ion population as a function of P_ϕ/ψ_1 and E with Λ=1. ψ_1 is the poloidal flux at the edge of the plasma. Top: T_{HOT} = 500 keV, Bottom: T_{HOT}= 1 MeV.

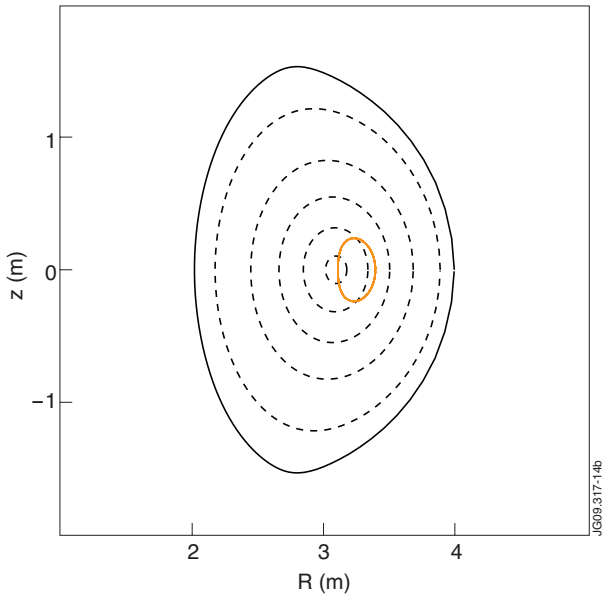

Figure 15: Poloidal projection of the orbits that maximizes the exchange of energy with the n=9 tornado mode. The orbit is the same both for T_{HOT} = 500keV and T_{HOT} = 1MeV and is defined by orbit defined by (E≈2.15 MeV, P_ϕ/ψ_1 ≈ −0.0015 and Λ=1).